AGU PUBLICATIONS

Geophysical Research Letters

RESEARCH LETTER
10.1002/2016GL070214

Key Points:
- Water vapor influences the dynamics of the cold sector of extratropical storms
- The cold sector poleward heat transport increases with humidity faster than that of the warm sector
- This reflects a more stable environment which supports stronger cold temperature anomalies

Supporting Information:
- Supporting Information S1

Correspondence to:
R. Geen,
rg419@exeter.ac.uk

Citation:
Geen, R., A. Czaja, and J. D. Haigh (2016), The effects of increasing humidity on heat transport by extra-tropical waves, *Geophys. Res. Lett.*, *43*, 8314–8321, doi:10.1002/2016GL070214.

Received 25 JAN 2016
Accepted 28 JUL 2016
Accepted article online 1 AUG 2016
Published online 15 AUG 2016

The effects of increasing humidity on heat transport by extratropical waves

Ruth Geen[1,2], Arnaud Czaja[1,2], and Joanna D. Haigh[1,2]

[1]Space and Atmospheric Physics Group, Department of Physics, Imperial College London, London, UK, [2]Grantham Institute, Imperial College London, London, UK

Abstract This study emphasizes the separate contributions of the warm and cold sectors of extratropical cyclones to poleward heat transport. Aquaplanet simulations are performed with an intermediate complexity climate model in which the response of the atmosphere to a range of values of saturation vapor pressure is assessed. These simulations reveal stronger poleward transport of latent heat in the warm sector as saturation vapor pressure is increased and an unexpected increase in poleward sensible heat transport in the cold sector. The latter results nearly equally from changes in the background stability of the atmosphere at low levels and changes in the temporal correlation between wind and temperature fields throughout the troposphere. Increased stability at low level reduces the likelihood that movement of cooler air over warmer water results in an absolutely unstable temperature profile, leading to less asymmetric damping of temperature and meridional velocity anomalies in cold and warm sectors.

1. Introduction

The imbalance between the distributions of insolation and outgoing longwave radiation requires that heat be transported poleward, driving both the Hadley cell and baroclinic eddies in the midlatitudes. As our world warms and the atmosphere holds more moisture, the balance and mechanisms involved will change, with more energy being carried in the form of latent heat [*Trenberth and Stepaniak*, 2003].

The importance of latent heat transport to the global energy budget can be seen by comparing the circulation on dry and moist isentropes. In the latter perspective, the mass fluxes are found to be twice as large [*Pauluis et al.*, 2008], indicating a strong latent heat flux. *Laliberté et al.* [2012] demonstrated that this difference arises from poleward and equatorward directed mass fluxes of similar dry potential temperature but different equivalent potential temperature. Air moves poleward with a higher moisture content and ascends on moist isentropes in the storm track. The return flow follows dry isentropes and is warmed and moistened by mixing in the boundary layer.

Eddy heat transport by the atmosphere dominates the midlatitude global energy flux [*Trenberth and Caron*, 2001] and has been demonstrated to be sensitive to climate [*O'Gorman and Schneider*, 2008]. Previous work has investigated the role of moisture either in zonal mean eddy heat transport [e.g., *Frierson et al.*, 2007; *Laliberté et al.*, 2012] or in development of individual systems [e.g., *Boutle et al.*, 2011; *Schemm et al.*, 2013], but how the two pictures connect is still unclear. For example, in a model with fixed optical depths and a mixed layer aquaplanet boundary condition, *Frierson et al.* [2007] found that as moisture was increased, the resulting increase in latent energy transport was compensated by a decrease in sensible heat transport. A diffusive energy balance model was used to interpret the importance of static stability, diffusivity coefficient, and emission level to this result, but the study did not examine the storm systems in which the heat is carried.

On a local scale, individual storms can be analyzed in terms of the behavior of the various air masses involved [e.g., *Browning and Roberts*, 1994]. The warm conveyor belt (WCB) is generally considered to be responsible for the majority of heat transport in a cyclone [*Eckhardt et al.*, 2004; *Madonna et al.*, 2014]. When only condensation and evaporation are considered as sources of diabatic heating, the WCB has been shown to strengthen in an idealized model for fixed initial conditions [*Schemm et al.*, 2013]. In an idealized baroclinic-wave simulation, *Boutle et al.* [2011] found that increasing the absolute temperature of the background state, and so altering the saturation vapor pressure, increased both storm eddy kinetic energy and moisture ventilation by the WCB and shallow convection, implying increased latent energy transport.

In the work detailed above much of the focus has been on the warm sector of the storm and its amplification when latent heating is included, with the assumption that this sector is the key to understanding the transports by the system. However, in a study of midlatitude poleward heat transport by extreme events in the ERA-Interim data set *Messori and Czaja* [2015] found that approximately 40% of these events are associated with equatorward movement of cooler air.

In the present study we relate changes in zonal mean eddy heat transport as moisture is increased to changes in the baroclinic systems which transport the heat. The latter have previously been investigated for fixed initial conditions, rather than in an equilibrated mean climate. Based on the effects of moisture on the WCB observed in previous work [e.g., *Schemm et al.*, 2013], it could be expected that as specific humidity is increased, the distribution of temperature perturbations in the midlatitudes should show fewer, stronger positive values, with the cold sector not directly affected. It would also be expected that more heat be transported as latent compared to sensible heat. In this paper, we investigate changes to both sectors of the storm by varying the moisture content of an intermediate complexity general circulation model (GCM). As predicted, stronger transport of latent heat is observed in moister climates. Unexpectedly, we further find that as moisture content increases, the increased background stability allows more negative temperature perturbations to develop. This results in stronger poleward heat transport by the cold sector.

2. Model and Data

We use the MIT General Circulation Model (MITgcm) [*Marshall et al.*, 1997a, 1997b], an intermediate complexity climate model. This is run as a hydrostatic aquaplanet atmosphere-only model on 25 equally spaced pressure levels. The primitive equations are solved on a cube-sphere with resolution C32, i.e., 32×32 points on each face. This corresponds to a resolution of roughly 2.8° at the equator [*Adcroft et al.*, 2004] and an average midlatitude grid spacing of approximately 280 km. Although this resolution is quite coarse, composites of extreme heat transport events (not shown) compare well with equivalent composites of events taken from the ERA-Interim reanalysis data set [*Messori and Czaja*, 2015]. The modeled storm systems have a clear WCB ascending and flowing poleward ahead of the cold front. In the cold sector, shallow convection ventilates moisture from the boundary layer. Additionally, *Booth et al.* [2013] found their results on the effects of moisture on storm enhancement to be robust even where individual fronts were not well resolved, although we note that our grid spacing is larger than the maximum they investigate (200 km).

With the exception of the optical depth parametrization, outlined in supporting information Text S1, and of the use of a roughness length of 5 cm for momentum, moisture, and sensible heat flux, the physics module is as detailed in *O'Gorman and Schneider* [2008] and is based on *Frierson et al.* [2006] and *Frierson* [2007], with the planetary boundary layer (PBL) diffusivity scheme of *Troen and Mahrt* [1986]. Sensitivity experiments confirm that the results presented here are not dependent on the choice of roughness length. Inspection of wind speed and temperature profiles (not shown) indicate that the model is capable of producing a semirealistic boundary layer structure. The model includes simple schemes to simulate moist convection and large-scale condensation of water vapor. Clouds are not parametrized, with condensate instead falling straight out. An approximate Clausius-Clapeyron equation is used with a constant latent heat of vaporization:

$$e_s = e_{s0} e^{-(L/R_v)[(1/T)-(1/T_0)]}. \tag{1}$$

In the above, e_s is the saturation vapor pressure, which is a function of temperature, T. e_{s0} is a reference value of 610.78 Pa for this at a reference temperature $T_0 = 273.16$ K. L is the latent heat of vaporization of water, taken to have a constant value of 2.5×10^6 J kg^{-1}, and R_v is the gas constant for water vapor. Following *Frierson et al.* [2006] and *Booth et al.* [2013], in order to explore the effect of varying moisture content on the eddy heat fluxes, the constant e_{s0} in equation (1) is multiplied by factors of 0, 0.1, 0.25, 0.5, 0.75, 1, 1.25, and 1.5. In what follows "dry" and "wet" refer to the simulations where factors of 0 and 1 are used, respectively. A factor of 1 corresponds to the relationship between temperature and humidity found in the real world. Factors less (greater) than 1 result in a smaller (larger) increase of humidity with temperature. This artificial method provides a controlled way to vary the moisture content of the atmosphere while holding other parameters in the model constant. Mechanisms for the influence of latent heat release on the circulation may then be explored.

The sea surface temperatures (SSTs) are fixed to the control profile from the Aquaplanet Experiment [*Neale and Hoskins*, 2001]. The top of atmosphere insolation used is as in *O'Gorman and Schneider* [2008], and we

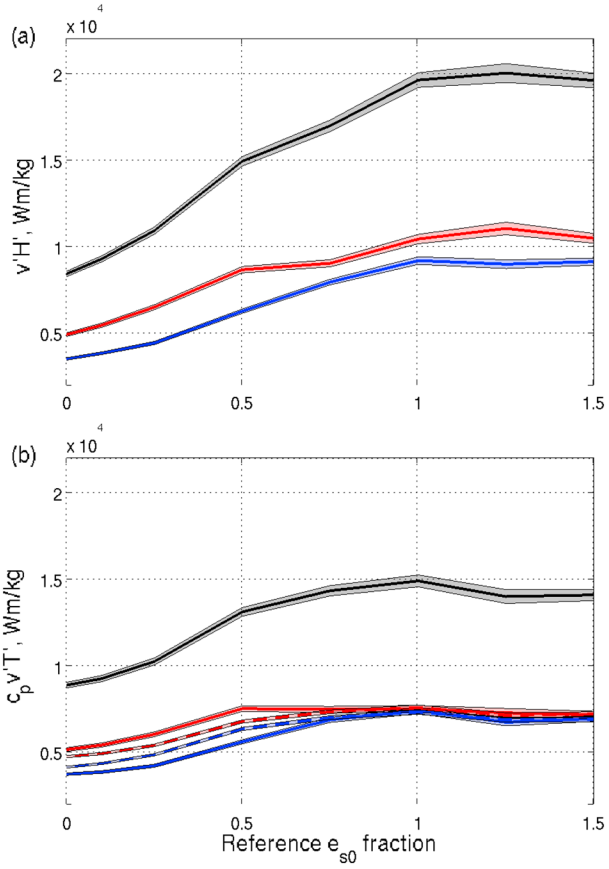

Figure 1. Zonal and temporal mean eddy transport of (a) moist static energy, (b) sensible heat, averaged from surface to tropopause at the latitude of strongest $\overline{v'T'}$, as a function of reference e_{s0} fraction. The black line indicates the total, and the red and blue show warm and cold sector contributions. Dashed lines indicate estimated transport, see section 3.3. Shaded areas indicate standard error, assuming data are uncorrelated after 10 days.

thus run in a perpetual equinox with no seasonal or diurnal cycle. Each model month is taken to be 30 days long, so that a year refers to a period of 360 days. With no seasonal cycle and the aquaplanet setup, all days and both hemispheres are equivalent, and the fixed SST means that the model equilibrates quickly. For each run discussed, the data used comprise daily snapshots taken from years 2 to 11 of the simulation, following one year of spin-up. All eddy quantities are defined as the instantaneous value of a field minus its temporal and zonal average at that location. Eddy quantities and temporal-zonal means will be indicated by primes and bars, respectively. "Heat transport" is defined to be positive poleward, with both poleward transport of warm air and equatorward transport of cooler air giving a positive heat flux.

In the experiments discussed here, we explore the effects of latent heat on heat transport. To separate these from the radiative effects, the model is run for 11 years for default e_{s0} (610.78 Pa) with the radiation scheme calculating optical depths from the water vapor content of the atmosphere. The temporal and zonal average of years 2 to 11 is then used to run the model with fixed optical depths. The radiation scheme may still respond to the instantaneous temperatures. This allows regions of the atmosphere to be warmed and cooled appropriately and a balanced energy budget to be maintained. The results below apply to these fixed optical depth simulations.

3. Results

3.1. Moist Static Energy Transport

The moist static energy, H, is evaluated as

$$H = c_p T + gz + Lq, \tag{2}$$

where the first two terms account for the dry static energy of an air parcel, and the final term accounts for the latent heat carried by the water vapor [*Neelin and Held*, 1987]. Figure 1a shows the pressure averaged zonal and temporal mean moist static eddy heat flux, $\overline{v'H'}$, across the latitude of maximum $\overline{v'T'}$ for each run, which we take as indicative of the storm track position. The black line indicates the total eddy heat flux, which is seen to increase with humidity. As the water vapor content of the model is increased, the resulting increase in latent heat release above the fixed SST leads to an increase in the imbalance between energy received and lost at high and low latitudes. Accordingly, the model shows an increase in poleward heat transport. We note, however, that our use of fixed SSTs does not permit a response by the ocean, and so this signal may not translate directly to the real world.

The red and blue lines in Figure 1a show the proportion of $\overline{v'H'}$ associated with positive and negative values of T', which are taken as representative of the warm and cold sectors of extratropical storms. It is noted that this type of temperature anomaly diagnostic does not capture the cold sector of the storm as well as diagnostics such as sensible heat flux, low-level static stability, or potential vorticity (PV) [e.g., *Vannière et al.*, 2016].

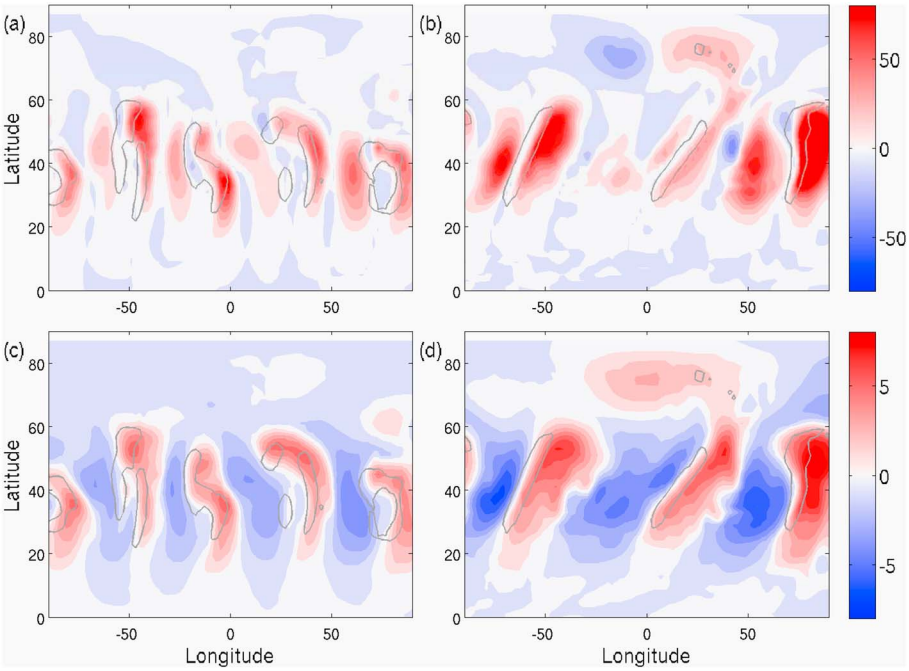

Figure 2. Snapshots of (a, b) $v'T'$, km/s, and (c, d) T', K, at 820 hPa for the (a, c) dry and (b, d) wet experiments. Grey contours represent an indicator of the position of the front calculated as the product of temperature gradient and relative vorticity at 980 hPa.

Caution must therefore be taken in relating the T' discussed here to more technical descriptions of cyclogenesis. However, v' and T', and their product, relate more directly to the transient eddy heat flux often discussed in the zonal mean heat budget. This method therefore provides a way to relate local variations in these fields and the mechanisms involved in these to larger scale average characteristics of the circulation.

Based on studies on the effect of latent heat release on the WCB [*Boutle et al.*, 2011; *Schemm et al.*, 2013], we expect the increase in total heat transport to come via increased latent and sensible heat transport in the warm sector of the storm and possibly some enhancement of the storm strength [*Boutle et al.*, 2011; *Booth et al.*, 2013]. As expected, we see a stronger eddy moist static energy flux in the warm sector, where the humidity is greater than in the drier cold sector. However, separating out the contribution from sensible heat flux, $c_p v'T'$, in Figure 1b we find that the cold sector transport of this quantity actually increases relative to the warm sector transport, moving from an approximately 60:40 to 50:50 split from the dry to wet simulations. For the simulations with e_{s0} above 1.0 there is no further change. It seems, surprisingly, that poleward heat transport in the cold sector of the storm has been enhanced by the increased water vapor content. Equivalently, the larger contribution of the warm sector to $\overline{v'H'}$ in Figure 1a is not only due to an increase in warm sector moist static energy transport with increased water vapor but also a weaker sensible heat transport by the cold sector at low saturation vapor pressure.

3.2. Sensible Heat Transport

Snapshots of T' and $v'T'$ at 820 hPa also suggest a change in the role of the cold sector in poleward heat transport between the dry and moist simulations. In the dry experiment, Figure 2a, we see that the eddy heat fluxes are strongest ahead of the cold front (see caption), in the warm sector of the storm. Comparing with the wet case, Figure 2b, we find agreement with the conclusions drawn from Figure 1b. As humidity increases, the $v'T'$ associated with the cold sector increases significantly, with regions of strong $v'T'$ now appearing behind the cold front.

Inspection in Figures 2c and 2d, showing T' for the dry and wet simulations, indicates that in the wet model warm and cold sectors of similar magnitude occur. However, in the dry model, we observe a tendency to find stronger warm than cold T', suggesting that an asymmetry between the warm and cold sectors in the dry model may be responsible for the weaker cold sector sensible heat flux. Although conclusions may not be drawn from these individual snapshots an analysis of the probability density functions of T' and v', shown in

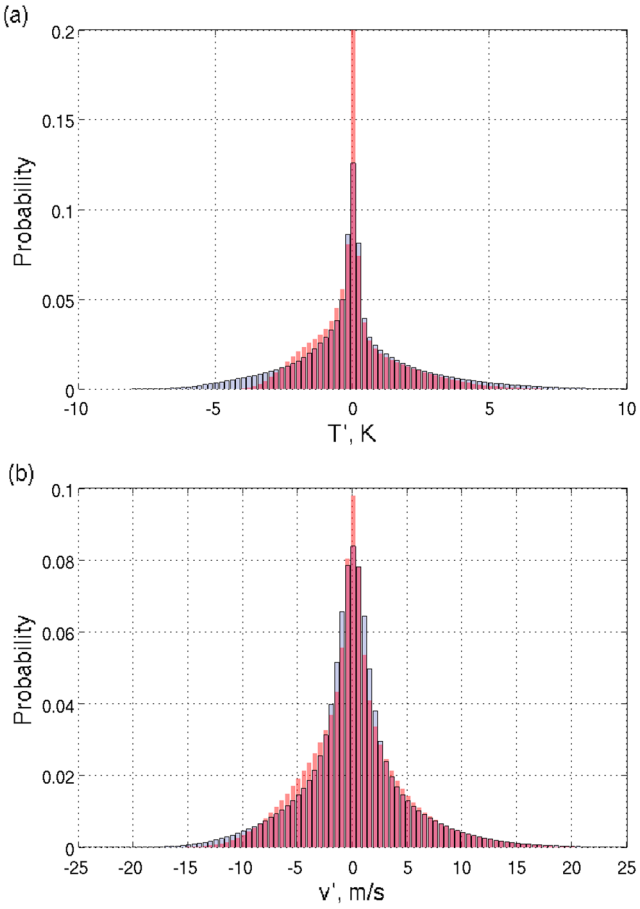

Figure 3. PDFs of (a) T' and (b) v' at 820 hPa. Dry run is shown in red and wet run in blue.

Figure 3, provides support for this hypothesis. These clearly demonstrate that the distribution of T' in the dry model is asymmetric compared to the wet, while the v' distributions are relatively symmetric.

It is also noted that Figure 2 indicates that the wavelength of the eddies increases as moisture increases in our simulation. In experiments using prescribed initial conditions, *Booth et al.* [2013] observed a strengthening and narrowing of ascent with moisture. In contrast, in Coupled Model Intercomparison Project phase 3 (CMIP3) global warming simulations *Kidston et al.* [2010] observed an increase in eddy length scale, as is seen here. One explanation for the different behavior may be the ability of the model mean state to evolve in our simulations. As humidity increases, the static stability of the atmosphere is also increased [e.g., *Juckes*, 2000; *Frierson et al.*, 2006], which may suppress the enhanced ascent observed by *Booth et al.* [2013].

Different physical processes drive and damp the wave in different atmospheric layers. To aid comparison of our experiments, we divide our atmosphere into two regions. In the first, an approximation to the PBL, interactions with the surface, diffusion, and shallow convection are expected to dominate. This layer is defined from the surface to the zonal mean of the PBL height used in the diffusion scheme [*Frierson et al.*, 2006]. Note that the PBL height decreases as moisture content, and thus static stability, increases. In the dry (wet) simulation, at the latitude of maximum $\overline{v'T'}$, the PBL on average encompasses seven (three) model layers, extending up to ~720 hPa (~880 hPa), with a mean height of ~2.6 km (~0.6 km) associated with negative T'. The second layer discussed, the free troposphere, extends from the top of the PBL to the tropopause, for which we use the World Meteorological Organization (WMO) definition, taking the tropopause height to be the lowest pressure level where the lapse rate reaches, and stays below, 2 K km^{-1}.

Figure 4a shows the variance of the eddy temperatures, $\overline{T'^2}$, associated with positive and negative T' in the PBL (dashed) and free troposphere (solid). The dashed line shows that, for all experiments, in the PBL greater variance is associated with positive rather than with negative values of T', indicating higher magnitude anomalies in the warm than cold sector of the storm in this layer. By contrast, equal warm and cold sector variance is found in the free troposphere. We may therefore attribute asymmetry between cold and warm sector T' magnitude to processes in the PBL. Equivalent plots of $\overline{v'^2}$ associated with positive and negative v' (Figure 4b) also show that the positive v' is stronger than the negative in the boundary layer, while in the free troposphere similar magnitudes are found. Understanding the boundary layer physics, and the control of moisture on this, appears to be a good starting point in interpreting the behavior seen in Figure 1.

3.3. Mechanism

While the PBL height differs between each experiment, becoming shallower as moisture content is increased, $\overline{T'^2}$ and $\overline{v'^2}$ averaged over the PBL model levels vary comparatively little as humidity increases, see Figure 4. In this layer, the warm sector is associated with larger $\overline{T'^2}$ than the cold sector, and positive anomaly $\overline{v'^2}$ is greater

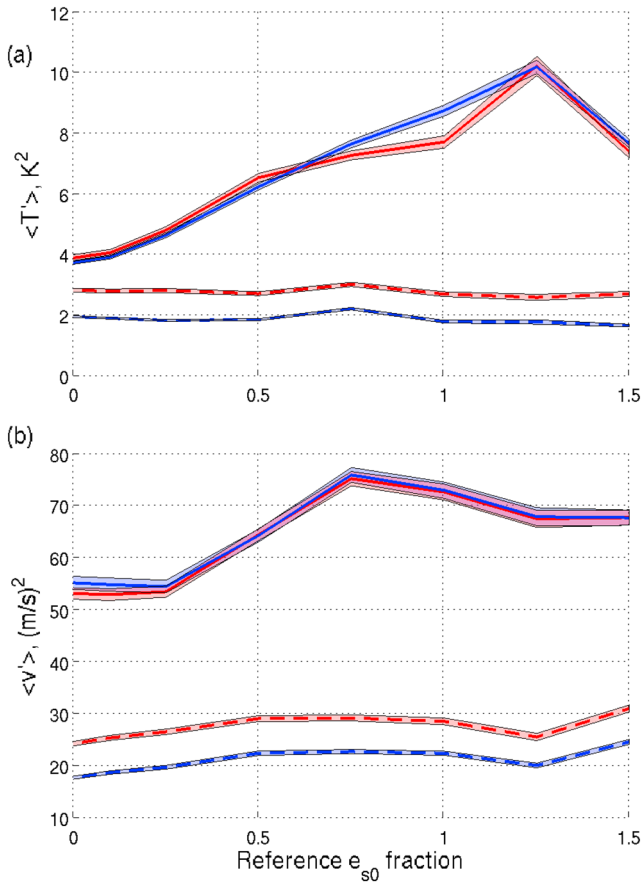

Figure 4. (a) As Figure 1 but for $\overline{T'^2}$ (total not shown). (b) As before but for $\overline{v'^2}$ and with red (blue) line indicating positive (negative) v'. Solid lines indicate pressure averages over the free troposphere, dashed lines averages over the boundary layer.

than negative anomaly $\overline{v'^2}$ for all experiments considered. The consistent behavior between the experiments suggests that a dry mechanism is responsible for the asymmetry.

In the PBL, the temperature and velocity fluctuations in the waves will be damped by diabatic and frictional effects, respectively. In MITgcm, the diabatic heating, Q, is composed of contributions from radiative heating, diffusive heating, convective heating, and heating due to large-scale condensation. To identify the component responsible for the asymmetric damping, we calculate an approximate damping coefficient, averaged over the PBL, by evaluating $\overline{Q'\theta'}/\overline{\theta'^2}$ for the warm and cold sectors of each run. The asymmetry appears predominantly driven by the diffusive heating, with the cold sector in the dry run damped by this term by -0.72 day^{-1}, compared to -0.56 day^{-1} for the warm sector. In the wet simulation this asymmetry is reduced, with diffusive heating damping the cold and warm sectors by -0.52 day^{-1} and -0.47 day^{-1}, respectively. From latitude-pressure distributions of the damping coefficient for the total diabatic heating, supporting information Figure S1, it can be seen that the cold sector is more strongly damped than the warm sector and that damping is strongest in the PBL.

The model's diffusive heating term is expressed:

$$Q_{\text{diff}} = \frac{\partial}{\partial z}\left(K\frac{\partial \theta}{\partial z}\right). \tag{3}$$

The diffusive heating is therefore related to both the curvature of the potential temperature profile and, through K [*Troen and Mahrt*, 1986], to the local dry stability of the atmosphere. Warm air will tend to be cooled and cold air warmed, with the magnitude of heating determined largely by the diffusion coefficient.

In each run, the tropics are close to moist neutrality, while the midlatitudes are generally observed to be more stable [*Juckes*, 2000; *Frierson et al.*, 2006]. In the cold sector of the storm cooler air is moved over warmer water, resulting in a less stable temperature profile. Particularly in the drier experiments, where mean state stability is low, the cold sector can become absolutely unstable, leading to a large model diffusion coefficient and strong warming of the cold air parcel. As humidity increases, the increase in background stability allows larger values of T' to be supported, and the role of the warm and cold sectors becomes more symmetric. Similarly, the diffusion coefficient for momentum is dependent on static stability so that motion will be damped more strongly in the cold than warm sector. Evaluating $\overline{F'v'}/\overline{v'^2}$, where F is the meridional momentum tendency due to vertical diffusion, confirms this. In the dry (wet) simulation the cold and warm sector v' are damped by -1.07 day^{-1} (-1.55 day^{-1}) and -0.82 day^{-1} (-1.29 day^{-1}), respectively.

Our stability related mechanism explains the features noted in the T' and v' variances in Figure 4. Positive values of $v'T'$ will be observed where v' and T' are both of the same sign, and so an increase in eddy heat

flux may be produced by an increase in the magnitude or in the degree of correlation between these. To quantify how much of the signal over the whole atmosphere is related to damping in the PBL, we estimate the contribution of this region to $\overline{v'T'}$ from the surface to the tropopause. Weighting the average of the cold and warm sector sensible heat fluxes in the free troposphere and the individual cold and warm sector fluxes from the PBL by their respective depths provides an estimate of how much of the signal in surface-to-tropopause $\overline{v'T'}$ is generated by changes to the PBL. This estimate is shown as the dashed line in Figure 1b. Taking the ratio of the difference between the estimates and actual values for the dry run, we find that 43% of the total signal can be explained by changes to the PBL height and the resulting changes to how diffusive heating damps eddy temperatures. The remainder of the signal would appear to arise from an increase in correlation between same sign v' and T' values.

4. Summary

We have shown that in an idealized model, increasing humidity not only changes the partitioning of midlatitude poleward heat transport between latent and sensible heat but also between the warm and cold sector of the storm. As expected we find an increase in the latent and sensible heat fluxes associated with the warm sector. However, we find additionally that the cold sector heat transport strengthens, accounting for 50% of the total increase in moist static energy transport and 61% of the increase in sensible heat transport between the dry and wet simulations seen in Figure 1. While in drier models the cold sector provides a proportionally smaller heat flux, this increases with humidity until the cold and warm sectors give a similar contribution.

The strengthening of the cold sector heat transport is partially explained by an increase in the magnitude and spread of negative values of T' with moisture. In the model PBL, cold T' values are strongly damped by diffusive heating, particularly when the temperature profile is unstable. As static stability increases with humidity, the modeled PBL depth decreases, allowing more of the atmosphere to support a stronger cold sector. Simply put, at lower levels, bringing warmer air masses over colder water yields a stable profile. By contrast bringing cooler air over warmer air or water, particularly in an environment already close to dry stable, can result in an absolutely unstable temperature profile which is quickly damped, limiting the strength of cold T' that can develop in the storm.

The remainder of the changes to the balance of warm sector versus cold sector poleward heat transport appear to be related to the correlation of the wind and temperature fields. While analysis of this feature is beyond the scope of this study, it is possible that this could relate to the enhanced PV that has previously been observed as moisture is increased in initial condition experiments [e.g., *Booth et al.*, 2013; *Schemm and Wernli*, 2014]. From the PV tendency equation it can be shown that an air parcel moving below a region of positive diabatic heating will undergo an increase in PV (see equation (2) [*Schemm and Wernli*, 2014]. This effect has been discussed in relation to storm strength [*Booth et al.*, 2013] and might also result in enhanced correlation between v' and T' throughout the system as the storm circulation increases.

Although WCBs may be a tempting starting point in understanding the feedbacks of water vapor on heat transport, significant heat fluxes are also associated with negative eddy temperatures. We have shown here that the strength and contribution of these to the total heat transport is sensitive to moisture, suggesting an additional feedback mechanism onto the midlatitude heat transport. Further investigation of this effect in higher resolution GCMs with more complete physics, or in reanalysis data, is needed to gauge the significance of this result. However, it suggests that there may be previously unexpected feedbacks on the cold sector and that research in this area, as well as in changes to the warm sector, is important in understanding the response of midlatitude heat transport to global warming.

Acknowledgments
Ruth Geen was funded by the Grantham Institute. Additional funds for mobility and consumables were provided by Climate-KIC. The data for the simulations discussed are available from the authors on request. The radiation scheme used is described in supporting information Text S1.

References

Adcroft, A., J.-M. Campin, C. Hill, and J. Marshall (2004), Implementation of an atmosphere-ocean general circulation model on the expanded spherical cube, *Mon. Weather Rev.*, *132*, 2845–2862.

Booth, J. F., S. Wang, and L. Polvani (2013), Midlatitude storms in a moister world: Lessons from idealised baroclinic life cycle experiments, *Clim. Dyn.*, *41*, 787–802.

Boutle, I. A., S. E. Belcher, and R. S. Plant (2011), Moisture transport in midlatitude cyclones, *Q. J. R. Meteorol. Soc.*, *137*, 360–373.

Browning, K. A., and N. M. Roberts (1994), Structure of a frontal cyclone, *Q. J. R. Meteorol. Soc.*, *120*, 1535–1557.

Eckhardt, S., A. Stohl, H. Wernli, P. James, C. Forster, and N. Spichtinger (2004), A 15-year climatology of warm conveyor belts, *J. Clim.*, *17*, 218–237.

Frierson, D. (2007), The dynamics of idealized convection schemes and their effect on the zonally averaged tropical circulation, *J. Atmos. Sci.*, *64*, 1959–1976.

Frierson, D., I. M. Held, and P. Zurita-Gotor (2006), A gray-radiation aquaplanet moist GCM. Part I: Static stability and eddy scale, *J. Atmos. Sci.*, *63*, 2548–2566.
Frierson, D., I. M. Held, and P. Zurita-Gotor (2007), A gray-radiation aquaplanet moist GCM. Part II: Energy transports in altered climates, *J. Atmos. Sci.*, *64*, 1680.
Juckes, M. N. (2000), The static stability of the midlatitude troposphere: The relevance of moisture, *J. Atmos. Sci.*, *57*, 3050–3057.
Kidston, J., S. M. Dean, J. A. Renwick, and G. K. Vallis (2010), A robust increase in the eddy length scale in the simulation of future climates, *Geophys. Res. Lett.*, *37*, L03806, doi:10.1029/2009GL041615.
Laliberté, F., T. Shaw, and O. Pauluis (2012), Moist recirculation and water vapor transport on dry isentropes, *J. Atmos. Sci.*, *69*, 875–890.
Madonna, E., H. Wernli, H. Joos, and O. Martius (2014), Warm conveyor belts in the ERA-Interim dataset (1979–2010). Part I: Climatology and potential vorticity evolution, *J. Clim.*, *27*, 3–26.
Marshall, J., A. Adcroft, C. Hill, L. Perelman, and C. Heisey (1997a), A finite-volume, incompressible Navier Stokes model for studies of the ocean on parallel computers, *J. Geophys. Res.*, *102*, 5753–5766.
Marshall, J., C. Hill, L. Perelman, and A. Adcroft (1997b), Hydrostatic, quasi-hydrostatic, and nonhydrostatic ocean modeling, *J. Geophys. Res.*, *102*, 5733–5752.
Messori, G., and A. Czaja (2015), On local and zonal pulses of atmospheric heat transport in reanalysis data, *Q. J. R. Meteorol. Soc.*, *109*, D02S07, doi:10.1029/2002JD003026.
Neale, R. B., and B. J. Hoskins (2001), A standard test for AGCMs including their physical parametrizations I: The proposal, *Atmos. Sci. Lett.*, *1*, 153–155, doi:10.1006/asle.2000.0019.
Neelin, J. D., and I. M. Held (1987), Modeling tropical convergence based on the moist static energy budget, *Mon. Weather Rev.*, *115*, 3–12.
O'Gorman, P. A., and T. Schneider (2008), The hydrological cycle over a wide range of climates simulated with an idealized GCM, *J. Clim.*, *21*, 3815–3832.
Pauluis, O., A. Czaja, and R. Korty (2008), The global atmospheric circulation on moist isentropes, *Science*, *321*, 1075–1078.
Schemm, S., and H. Wernli (2014), The linkage between the warm and the cold conveyor belts in an idealized extratropical cyclone, *J. Atmos. Sci.*, *71*, 1443–1459.
Schemm, S., H. Wernli, and L. Papritz (2013), Warm conveyor belts in idealized moist baroclinic wave simulations, *J. Atmos. Sci.*, *70*, 627–652.
Trenberth, K. E., and J. M. Caron (2001), Estimates of meridional atmosphere and ocean heat transports, *J. Clim.*, *14*, 3433–3443.
Trenberth, K. E., and D. P. Stepaniak (2003), Covariability of components of poleward atmospheric energy transports on seasonal and interannual timescales, *J. Clim.*, *16*, 3691–3705.
Troen, I., and L. Mahrt (1986), A simple model of the atmospheric boundary layer; sensitivity to surface evaporation, *Boundary Layer Meteorol.*, *37*, 129–148.
Vannière, B., A. Czaja, H. Dacre, T. Woollings, and R. Parfitt (2016), A potential vorticity signature for the cold sector of winter extratropical cyclones, *Q. J. R. Meteorol. Soc.*, *142*, 432–442.